Structural arrangement of the transmission interface in the antigen ABC transport complex TAP

Giani Oancea[a], Megan L. O'Mara[b], W. F. Drew Bennett[b], D. Peter Tieleman[b], Rupert Abele[a], and Robert Tampé[a,1]

[a]Institute of Biochemistry, Biocenter, Johann Wolfgang Goethe-Universität, Max-von-Laue-Strasse 9, D-60438 Frankfurt/Main, Germany; and [b]Department of Biological Sciences, University of Calgary, 2500 University Drive NW, Calgary, Alberta, Canada T2N 1N4

Edited by H. Ronald Kaback, University of California, Los Angeles, CA, and approved February 3, 2009 (received for review November 6, 2008)

The transporter associated with antigen processing (TAP) represents a focal point in the immune recognition of virally or malignantly transformed cells by translocating proteasomal degradation products into the endoplasmic reticulum–lumen for loading of MHC class I molecules. Based on a number of experimental data and the homology to the bacterial ABC exporter Sav1866, we constructed a 3D structural model of the core TAP complex and used it to examine the interface between the transmembrane and nucleotide-binding domains (NBD) by cysteine-scanning and cross-linking approaches. Herein, we demonstrate the functional importance of the newly identified X-loop in the NBD in coupling substrate binding to downstream events in the transport cycle. We further verified domain swapping in a heterodimeric ABC half-transporter complex by cysteine cross-linking. Strikingly, either substrate binding or translocation can be blocked by cross-linking the X-loop to coupling helix 2 or 1, respectively. These results resolve the structural arrangement of the transmission interface and point to different functions of the cytosolic loops and coupling helices in substrate binding, signaling, and transport.

membrane protein structure | traffic ATPase | substrate recognition | conformational change | cysteine cross-linking

The transporter associated with antigen processing (TAP) represents a key machinery in MHC class I antigen presentation by translocating proteasomal degradation products into the lumen of the endoplasmic reticulum (ER) for loading onto MHC class I molecules. Kinetically stable peptide–MHC complexes overcome the ER quality control and subsequently traffic to the cell surface, where they are inspected by $CD8^+$ cytotoxic T lymphocytes, which allows for an efficient discrimination of virus-infected or malignantly transformed cells (see refs. 1–3 for review).

TAP belongs to the ABC transporter family, which translocates a diverse spectrum of solutes across membranes driven by ATP binding and hydrolysis (4–7). TAP forms a heterodimeric complex composed of TAP1 and TAP2. Each half-transporter consists of a transmembrane domain (TMD) and a cytosolic nucleotide-binding domain (NBD), which binds and hydrolyzes ATP. Based on structural and biochemical data, the NBDs dimerize in the presence of ATP in a head-to-tail orientation, in which the 2 ATP molecules are complexed at the dimer interface (8–12). Each ATP-binding site is characterized by the Walker A and B motif completed by the C-loop of the opposite NBD.

TAP can be structurally and functionally dissected into a core transport complex composed of 2×6 transmembrane (TM) helices, which frame the peptide-binding pocket and translocation pathway, and a unique N-terminal domain (TMD0) per subunit, which is essential for tapasin binding and the assembly of a macromolecular MHC class I peptide-loading complex composed of TAP1, TAP2, tapasin, ERp57, calreticulin, MHC heavy chain, and β_2-microglobin (13–16).

The transport mechanism is composed of an ATP-independent peptide-binding and an ATP-dependent translocation step (17). Peptide transport and ATP hydrolysis are tightly coupled, implying a cross-talk between the TMDs and NBDs (18). A discrete peptide-binding region has been mapped within the core transport complex; it comprises the cytosolic loop 2 (CL2), which connects TM4 and TM5, as well as a stretch of 15 residues following TM6 (19). In addition, a peptide sensor site has recently been identified in CL1 of TAP1 (CL connecting TM2 and TM3), which transmits a bound peptide and subsequent translocation events via interdomain communication (20). Peptide binding induces a structural reorganization of the TAP complex, most likely via the transmission interface between the TMDs and NBDs (21).

To date, no high-resolution structure of any eukaryotic ABC transporter has been solved. However, x-ray structures of 2 bacterial ABC exporters, Sav1866 from *Staphylococcus aureus* and MsbA from *Salmonella typhimurium*, revealed an enlarged transmission interface comprising TM helix-extended CLs, which are able to reach across and contact the X-loop of the NBD of the opposite subunit by coupling helices (22, 23). However, the functional importance of this transmission interface and, in particular, its spatiotemporal organization during the transport cycle is presently unclear.

To examine the functional relevance of the transmission interface and domain swapping in a heterodimeric ABC half-transporter complex, we substituted the conserved glutamate of the newly identified X-loop of TAP2. By cysteine-scanning mutagenesis of CL1 and 2 of TAP1, we demonstrated close contacts between the X-loop and coupling helices 1 and 2 of the opposite half-transporter. The cross-linked transport complex can be reversibly arrested in a conformation incompetent in solute binding or translocation.

Results

Transmission Interface of the TAP Complex. An accurate coordination of the transport cycle of ABC transporters requires a spatiotemporal communication between distinct events in the TMDs and NBDs. For example, the presence of bound solute must be transmitted to the NBDs, which subsequently induce conformational changes by NBD dimerization, driving solute translocation across the membrane via conformational changes in the TMDs (18, 20). To define residues of the transmission interface in TAP, we constructed a 3D homology model of the core TAP complex based on the x-ray structure of Sav1866 (22). The final TAP model had a backbone root-mean-square deviation (RMSD) of 3.08 Å from the Sav1866 structure. The quality of the TAP1/2 model was

Author contributions: R.A. and R.T. designed research; G.O. performed research; G.O. contributed new reagents/analytic tools; G.O., M.L.O., W.F.D.B., D.P.T., R.A., and R.T. analyzed data; M.L.O., W.F.D.B., and D.P.T. performed modelling, model refinement and evaluation; and R.A. and R.T. wrote the paper.

The authors declare no conflict of interest.

This article is a PNAS Direct Submission.

Freely available online through the PNAS open access option.

Data deposition: The sequences in this paper has been deposited in the UniProt Knowledgebase, www.uniprot.org [accession numbers: Q03518/9, human TAP1/2 (ABCB2/3); Q9NP78, human TAPL (ABCB9); P08183, human MDL1 (ABCB1); P63359, *S. typhimurium* MsbA; and Q99T13, *S. aureus* Sav1866].

[1]To whom the correspondence should be addressed. E-mail: tampe@em.uni-frankfurt.de.

This article contains supporting information online at www.pnas.org/cgi/content/full/0811260106/DCSupplemental.

BIOCHEMISTRY

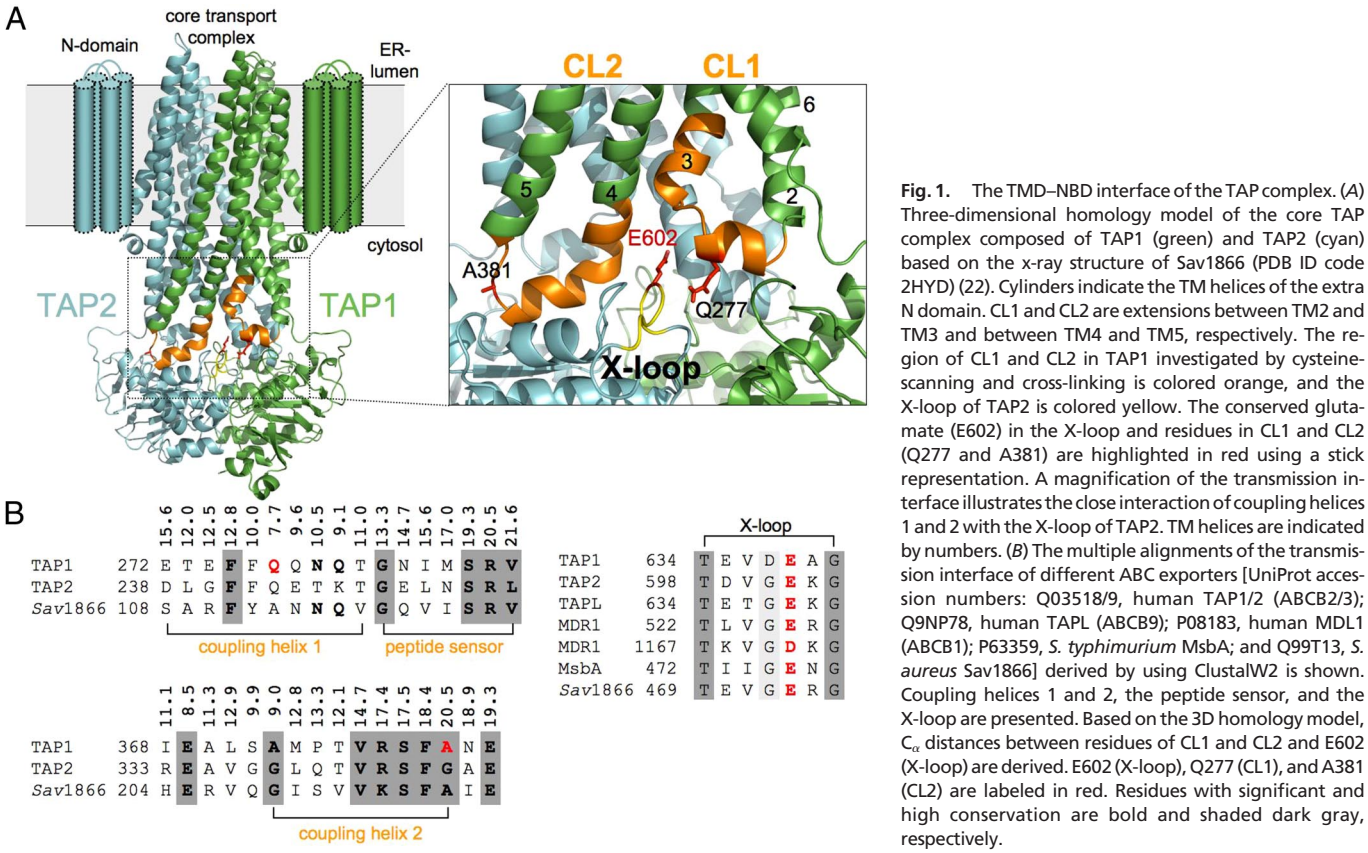

Fig. 1. The TMD–NBD interface of the TAP complex. (*A*) Three-dimensional homology model of the core TAP complex composed of TAP1 (green) and TAP2 (cyan) based on the x-ray structure of Sav1866 (PDB ID code 2HYD) (22). Cylinders indicate the TM helices of the extra N domain. CL1 and CL2 are extensions between TM2 and TM3 and between TM4 and TM5, respectively. The region of CL1 and CL2 in TAP1 investigated by cysteine-scanning and cross-linking is colored orange, and the X-loop of TAP2 is colored yellow. The conserved glutamate (E602) in the X-loop and residues in CL1 and CL2 (Q277 and A381) are highlighted in red using a stick representation. A magnification of the transmission interface illustrates the close interaction of coupling helices 1 and 2 with the X-loop of TAP2. TM helices are indicated by numbers. (*B*) The multiple alignments of the transmission interface of different ABC exporters [UniProt accession numbers: Q03518/9, human TAP1/2 (ABCB2/3); Q9NP78, human TAPL (ABCB9); P08183, human MDL1 (ABCB1); P63359, *S. typhimurium* MsbA; and Q99T13, *S. aureus* Sav1866] derived by using ClustalW2 is shown. Coupling helices 1 and 2, the peptide sensor, and the X-loop are presented. Based on the 3D homology model, C_α distances between residues of CL1 and CL2 and E602 (X-loop) are derived. E602 (X-loop), Q277 (CL1), and A381 (CL2) are labeled in red. Residues with significant and high conservation are bold and shaded dark gray, respectively.

assessed by using WHATIF on local factors, such as backbone conformation, bond lengths, side-chain planarity, and overall packing quality, and was found to be comparable with that of Sav1866. However, some caveats must be applied when using WHATIF for analysis of TM proteins (24). Therefore, we performed an additional analysis of the Ramachandran plot by using Swiss-PdbViewer (25). The Ramachandran plot showed that 99% of all TAP residues fell within favorable regions, increasing our confidence in the backbone geometry. The CLs of TAP and Sav1866 are of similar length and clearly distinct from the short intracellular loops of ABC importers (Fig. 1*A*).

The constructed model is in full agreement with a number of experimental data: (*i*) the membrane topology (26) and the identified core transport complex match perfectly the homology model (13), (*ii*) the peptide-binding pocket concurs with CL2 (19), and (*iii*) the sensor loop in CL1 is optimally positioned adjacent to the peptide-binding site (20) [see supporting information (SI) Fig. S1]. In the 3D model, the NBDs are close together with distances reflecting the ATP-bound state and the TMDs opened to the ER–lumenal site, reflecting an outward-facing conformation. The CLs are composed of TM extended helices, which are connected by short coupling helices in parallel orientation to the membrane plane (Fig. 1*A*). The X-loop of TAP occupies a central position, in which the conserved glutamate is surrounded by residues of CL1 and CL2 of the opposite subunit. The X-loop is localized in the α-helical domain of the NBD close to the C-loop, suggesting a role in transmitting conformational changes generated by ATP binding and hydrolysis. The sequence conservation of CL1 and CL2 including coupling helix 1, the identified peptide sensor and coupling helix 2, the X-loop as well as the C_α distances between the CLs, and the X-loop are shown in Fig. 1*B*.

Function of the X-loop in Peptide Translocation. Based on the peptide sensor identified in CL1 next to coupling helix 1 of TAP1 (20) and the sequence conservation of the X-loop in TAP2 (Fig. 1*B*), we focused on the interaction and interdomain communication between the X-loop of TAP2 and the CLs of TAP1. We first replaced the conserved glutamate (E602) in Cys-depleted TAP2 with aspartate, alanine, cysteine, and arginine, respectively. The X-loop mutants were coexpressed with Cys-less TAP1 at similar levels in insect cells (Fig. 2*A*). Importantly, peptide binding to TAP was not affected, demonstrating that the X-loop mutations did not interfere with membrane insertion, folding, or heterodimer assembly. Remarkably, the X-loop mutations showed a reduced transport activity, with 50% transport activity for E602C and 20% for E602D or E602A (Fig. 2*B*). Complete disruption of peptide transport was observed for the E602R mutant. Thus, the conserved glutamate in the X-loop plays an important role in the translocation event but not in substrate binding.

Functional Differences in CL1 and CL2. To identify residues involved in interdomain signaling, we applied a cysteine-scanning approach in CL1 and CL2 of TAP1. Based on the 3D model, we chose residues that frame the X-loop of TAP2 (Fig. 1). Altogether, 24 single-cysteine TAP1 mutants were coexpressed with TAP2(E602C) and yielded similar expression levels (Fig. 3*A*). Similar to the X-loop, mutations in the CL1, including coupling helix 1, did not significantly affect peptide binding. The slight differences correlated with alterations in the expression level. Remarkably, all mutations in coupling helix 1, except for Q277C, interfered with the transport activity. In addition, mutations in the peptide sensor region (G282C, I284C, and R287C) drastically decreased the transport activity. Strikingly, a different pattern is observed for mutations in CL2, which comprises the peptide-binding pocket (19, 27). Only R378C showed a significant decrease in peptide binding and transport (Fig. 3*B*). In addition, P375C of TAP1 strongly influenced peptide transport, whereas peptide binding was not affected. On average, CL2 is more tolerant to mu-

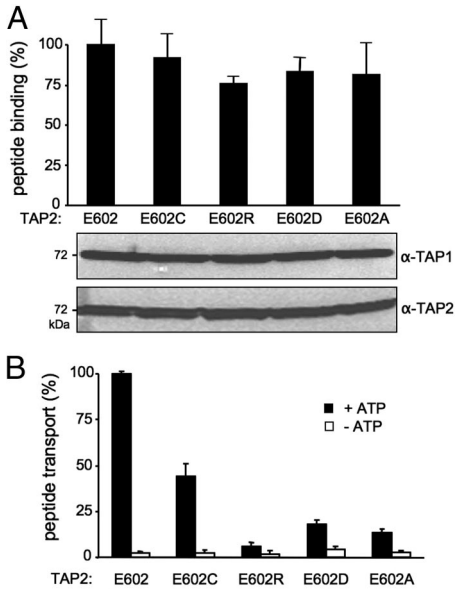

Fig. 2. Function of the glutamate in the X-loop of TAP2 in the allosteric coupling between peptide binding and translocation. (*A*) Peptide binding of X-loop mutants of TAP2. TAP-containing membranes (35 μg of protein) were incubated with 1 μM radio-labeled RRYQKSTEL for 15 min at 4 °C. Unspecific binding was determined in the presence of an excess of RRYQKSTEL (200 μM). The lower portion shows the expression level of X-loop mutants analyzed by 10% SDS/PAGE (20 μg of protein per lane) followed by immunoblotting against TAP1 (mAb 148.3) and TAP2 (mAb 435.3). (*B*) Peptide transport of X-loop mutants of TAP2. TAP-containing membranes (150 μg of protein) were incubated with fluorescein-labeled peptide [1 μM RRYQNSTC$^{(F)}$L] for 5 min at 32 °C in the presence (black bars) or absence (white bars) of 3 mM ATP. After lysis, N-core-glycosylated and thus translocated peptides were bound to ConA-beads and quantified by fluorescence detection after elution with methyl-α-D-mannopyranoside. Peptide binding and transport of TAP1(Cys-less)/TAP2(E602) was normalized to 100%. Data were collected from 3 independent experiments. The error bars represent the standard deviation.

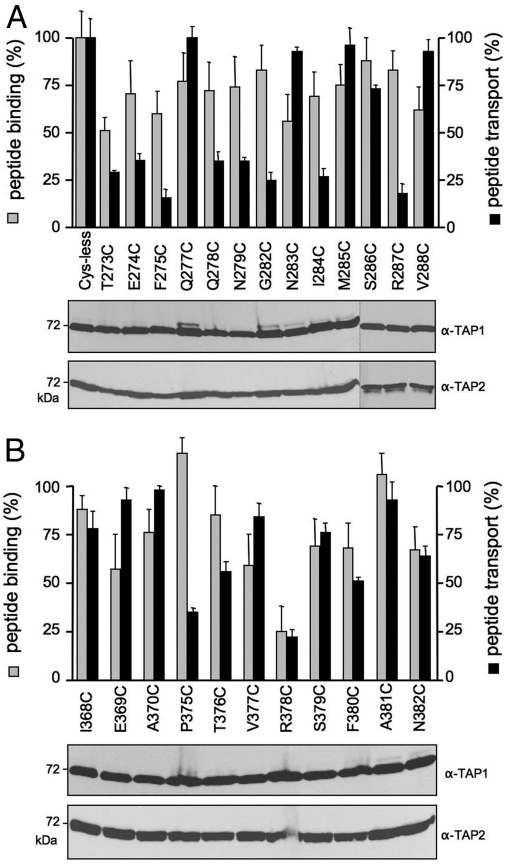

Fig. 3. CL1 and CL2 of TAP1 have distinct functions in peptide binding and translocation. Single-cysteine TAP1 mutants of CL1 (*A*) or CL2 (*B*) in complex with E602C(TAP2) were analyzed for peptide binding (gray bars) and transport (black bars). Peptide binding and transport were performed as described in the legend of Fig. 2. Specific peptide binding and transport of TAP1(Cys-less)/TAP2(E602C) was normalized to 100%. Data were collected from 3 independent experiments. The error bars represent the standard deviation. Equal amounts of TAP1 and TAP2 were confirmed by immunoblotting.

tagenesis than CL1 (82% vs 38% of mutations had no effect in transport). In conclusion, CL1 and CL2 have distinct functions in peptide binding and transport.

Domain Intertwining in the TAP Complex. We next analyzed contact sites between the CLs of TAP1 and the X-loop of TAP2 by oxidative cysteine cross-linking. This approach (28) was very productive in exploring the structure and function of *E. coli* lactose permease, human cystic fibrosis TM conductance regulator (CFTR), and P-glycoprotein (P-gp) (29–32). TAP cross-linking conditions using copper phenanthroline (CuPhe) were established for the A381/E602C complex (Fig. 4*A* and Fig. S2). The cysteine of TAP1 is located in CL2 and influences neither peptide binding nor transport. Cross-linking was performed on ice to limit thermal deactivation and structural dynamics of the TAP complex. The reaction was quenched after 1 min. Prolonged reaction time did not enhance the cross-linking efficiency because of the formation of sulfhydryl oxoforms (33). Interestingly, double bands at 162/174 kDa and 150/162 kDa were observed for TAP1 and TAP2, respectively. Single-cysteine TAP subunits, expressed alone, yielded a single band of 174 and 150 kDa for TAP1 and TAP2, respectively, indicating the formation of homodimeric complexes (34, 35). These homodimers, which form when one subunit is in excess (35), are most likely misfolded and thus inactive in peptide binding and translocation (17, 25). This finding is in line with the observation that single cysteines placed in each X-loop can be cross-linked in the homodimer but not in the heterodimer (data not shown). TAP2 variants with single intrinsic cysteines (C197, C208, and C213) in combination with Cys-less or A381C TAP1 did not lead to cross-linked homo- or heterodimers (Fig. S2). Cross-linking is reversible because only monomeric TAP subunits were observed under reducing conditions (data not shown). These findings demonstrate the specificity of the cross-linking between the X-loop (E602C) of TAP2 and CL1/2 of TAP1.

To examine the distance of the CLs and the X-loop, thereby verifying the domain intertwining, we performed cysteine-scanning and cross-linking experiments. Surprisingly, most of the positions in CL1 of TAP1 led to specific cross-linking with the X-loop of TAP2 with varying efficiency, demonstrating a flexible TMD–NBD interface (Fig. 4*B* and Fig. S3). Strong cross-linking was observed for residues of the C-terminal end of coupling helix 1 as well as the N-terminal half of the peptide sensor. In contrast, in CL2 we detected strong cross-links with the X-loop only for residues 368, 375, 380, and 381 (Fig. 4*C* and Fig. S3). This result indicates that interactions between the X-loop of TAP2 and CL2 of TAP1 are defined, in contrast to CL1. Similar cross-link patterns were obtained at 4 °C and 37 °C for all mutants (data not shown). The cross-link pattern did not change significantly at various stages of the transport cycle (e.g., bound ATP, ADP, peptide or viral inhibitor ICP47) (Fig. S4). Thus, CL1 appears to be highly dynamic, given that contacts can still occur between residues over C_α distances of up to 20.5 Å (Fig. 1*B*). In conclusion, these data demonstrate that the CLs of TAP1 interact with the X-loop of

BIOCHEMISTRY

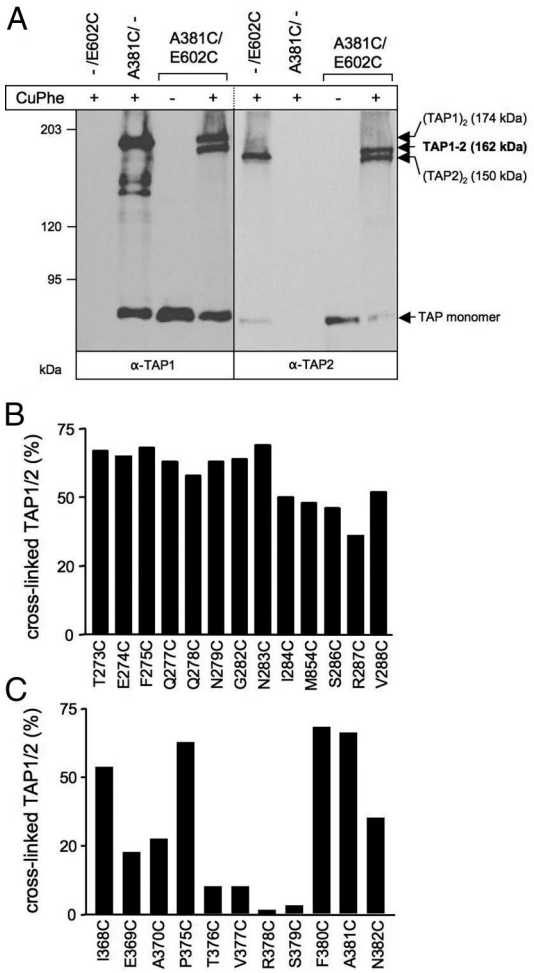

Fig. 4. Cysteine cross-linking between the CLs of TAP1 and the X-loop of TAP2. (*A*) Oxidative cysteine cross-linking of TAP1(A381C)/TAP2(E602). TAP-containing membranes (500 μg of protein) were incubated in the presence or absence of 1 mM CuPhe for 1 min at 4 °C. Samples were subjected to nonreducing 6% SDS/PAGE (20 μg of protein per lane) followed by immunoblotting against TAP1 and TAP2. The positions of the cross-linked TAP1–TAP2 (highlighted in bold), homodimeric $(TAP1)_2$ and $(TAP2)_2$, as well as monomeric TAP1 and TAP2 are indicated. (*B* and *C*) The cross-linking of the single-cysteine mutants of CL1 (*B*) and CL2 (*C*) in TAP1 with E602C of TAP2. The conditions are identical as described above. The efficiency of TAP1–TAP2 cross-linking was derived from TAP2 immunoblots.

TAP2, providing direct evidence for domain intertwining in heterodimeric ABC half-transporters.

Arresting the Transport Cycle by Cross-Linking. ABC exporters, including TAP, undergo multiple conformational changes during the transport cycle (5, 20, 21, 23, 36). However, due to the motional freedom of the CLs investigated herein, differences in cross-linking could not be resolved during the transport cycle (Fig. S4). Therefore, we investigated the interdomain communication by arresting TAP function via cysteine cross-linking. We chose 2 pairs of mutations, Q277C/E602C and A381C/E602C, containing a single cysteine in each coupling helix of TAP1. Importantly, these CL mutations neither affected peptide binding nor transport (see Fig. 3) but instead exhibited high cross-linking efficiency with the X-loop (Fig. 5). Strikingly, cross-linking of the A381C/E602C complex impeded both peptide binding and transport, in contrast to the combination with Cys-less TAP1 (Fig. 5*B*). Surprisingly, cross-linking of Q277C/E602C arrested TAP in a translocation-incompetent state, in which peptide binding was unaffected (Fig. 5*C*). The transport activity of Cys-less/E602C is only slightly reduced due to irreversible oxidation. Most importantly, the transport activity was fully restored by reduction of the disulfide bond, indicating that the cross-linking did not lead to an irreversible misfolding and dead-end pathway. In conclusion, CL2/X-loop cross-linking inactivates the peptide-binding site, and thus peptide translocation, whereas CL1/X-loop cross-linking disrupts the interdomain communication and prevents the structural rearrangements necessary for completion of the TAP substrate transport cycle after peptide binding.

Discussion

Peptide binding, transport, and ATP hydrolysis are tightly coordinated in the antigen transport complex TAP, implying an allosteric communication and signal transduction at the TMD–NBD interface (18, 20). In addition to the Q-loop, the newly identified X-loop in ABC exporters was proposed to be involved in this cross-talk (22). By substitution of the conserved glutamate in the X-loop of TAP2, we first demonstrated that the X-loop is indeed essential for the coupling of substrate binding to the subsequent translocation step. We further identified critical residues and contact sites in the CLs, thereby providing direct evidence for domain intertwining in a heterodimeric ABC transport complex. Cross-linking of the X-loop to coupling helix 1 arrests the TAP complex in a translocation-incompetent state, whereas cross-linking to coupling helix 2 inhibits substrate binding and thereby translocation.

The conserved glutamate in the X-loop is important for TAP function, because peptide transport is strongly impaired by substitution with a positively charged residue. The introduction of a short hydrophobic side chain or the conservative mutation to aspartate reduced transport activity to 20%, whereas substitution to cysteine decreased transport activity by only 50%. The reduced side chain of aspartate may position the negative charge in a disfavored environment. The sulfhydryl group of cysteine is largely tolerated. The X-loop appears very flexible because it shows a high B-factor in the x-ray structure of ABC exporters as well as of isolated NBDs (11, 37). We suggest that this region transmits ATP binding and hydrolysis of the NBDs to the TMDs via structural changes due to its close proximity to the C-loop, which senses the γ-phosphate of the bound ATP in the NBD–NBD interface. Remarkably, the RSMD of the C_α atom of the X-loop glutamate in the nucleotide-free and the ATP-bound state of HlyB-NBD is 3-fold higher than of the entire NBD (11, 38). However, it should be pointed out that the glutamate of the X-loop is conserved only in ABC subfamilies B and C. Whether this region is also part of the transmission interface in the other subfamilies remains to be addressed in future studies.

A surprising outcome of this study is that CL1 and CL2 have different functions. CL1 is important for the allosteric coupling of substrate binding and the subsequent transport event, whereas CL2 seems to function as an anchor via its coupling helix 2 and is part of the peptide-binding pocket. The 3D model suggests that the bulky hydrophobic phenylalanine residues of coupling helix 1 (F275 and F276) point into a hydrophobic core, thus stabilizing CL1, and substitution of these residues may collapse coupling helix 1. Mutations of hydrophilic and charged residues probably affect the orientation of CL1 or disrupt interdomain contacts. The function of CL1 in peptide sensing and allosteric coupling to the ATP-hydrolysis cycle was proposed recently, with residue 288 of TAP1 found to be in direct contact with the bound peptide; in addition, it was proposed that this sensor region is structurally reorganized during the transport cycle (20). Thus, the presence of a bound solute may be communicated via the adjacent coupling helix 1 to other parts of the protein responsible for completion of the transport cycle.

The structure of adenosine 5′-[β,γ-imido]triphosphate-bound and ADP-vanadate MsbA [Protein data bank (PDB) ID codes 3B60 and 3B5Z, respectively] closely correlates to the structure of

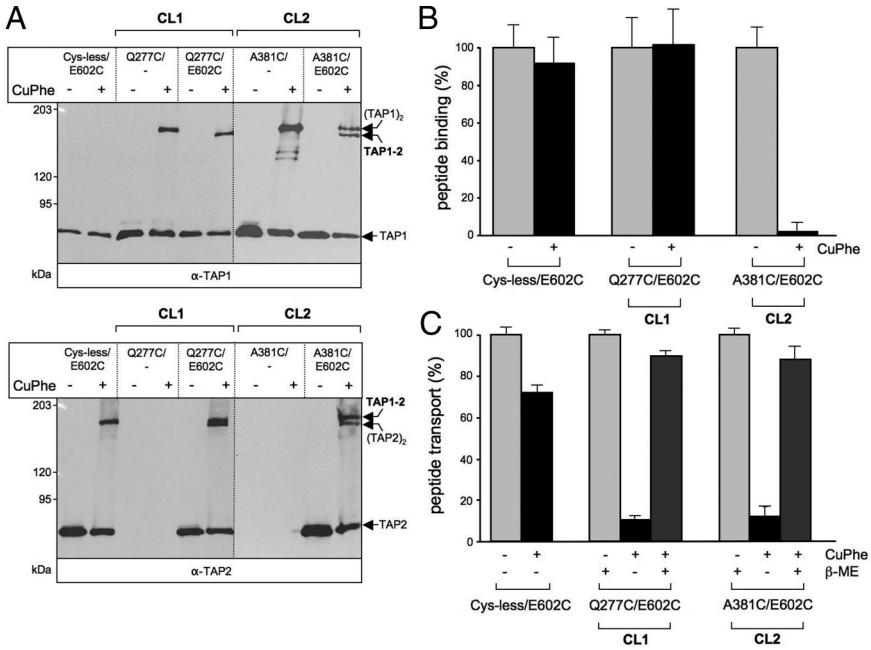

Fig. 5. Cysteine cross-linking inhibits peptide binding or translocation. Membranes (500 μg of protein) containing variants of TAP1 in combination with TAP2(E602C) were incubated in the presence or absence of CuPhe for 1 min at 4 °C. (*A*) Samples (20 μg of protein per lane) were analyzed by nonreducing 6% SDS/PAGE and immunoblotting. (*B*) Peptide binding to TAP treated with (black bars) or without (gray bars) CuPhe. TAP-containing membranes (35 μg of protein) were incubated with radio-labeled RRYQKSTEL (1 μM) at 4 °C for 15 min. Unspecific binding was determined in the presence of an excess of RRYQKSTEL (200 μM). Peptide binding to TAP in the absence of CuPhe was normalized to 100%. (*C*) Peptide transport via TAP treated with (black bars) or without (gray bars) CuPhe. TAP-containing membranes (150 μg of total protein) were incubated with fluorescein-labeled RRYQNSTC$^{(F)}$L (1 μM) for 5 min at 32 °C in the presence or absence of 3 mM ATP. To show reversibility, cross-linked samples were subsequently reduced with 100 mM 2-ME for 5 min at 4 °C (dark gray). ATP-dependent TAP transport activity in the absence of CuPhe was normalized to 100%. Data were collected from 3 independent experiments. The error bars represent the standard deviation.

Sav1866 (PDB ID code 2HYD) (22, 23). Because the Sav1866 crystal structure is at higher resolution, we chose to use only this structure as a modeling template for an ATP-bound conformation of TAP. To give an idea of possible TAP conformations, we have also threaded the sequence of TAP1 and TAP2 onto 3 of the C_α MsbA structures: ADP-vanadate trapped (PDB ID code 3B5Z), closed apo conformation (PDB ID code 3B5X), and open apo conformation (PDB ID code 3B5W). Comparison of the TAP models shows that the distance between the C_α atoms of the CL1 residue 277 and the X-loop residue 602 increases from 7.0 Å in the ATP-bound state to 26.5 Å in the apo closed state and 63.1 Å in the apo open state (Table S1). Covalent modification of these residues by cysteine cross-linking would prevent the structural rearrangements necessary for the transport cycle. These distances from the Sav1866- and MsbA-based models support the experimental results that CL1/X-loop cross-linking disrupts interdomain communication and prevents the structural rearrangements necessary for completion of the substrate transport cycle, whereas substrate binding is not affected.

Comparison of the TAP homology models in the apo open and closed conformation and the ATP-bound conformation showed that the distance between CL2 and the X-loop did not vary significantly throughout the transport cycle (Table S1). This model is supported by the CL2/X-loop cross-linking efficiency, which did not vary throughout the catalytic cycle. By using peptide photo-cross-linking and deletion studies, the region comprising CL2 was previously identified as part of an overlapping peptide-binding region (19, 27). Here, we could demonstrate that R378 in TAP1 is essential for peptide binding. The 3D model indicates that this residue is part of coupling helix 2. Its side-chain points into the opposite direction of the X-loop and might stay in direct contact with the peptide. It is tempting to speculate that the positive guanidinium group forms a salt bridge with the C-terminal carboxyl group of the peptide, which is essential for recognition. Interestingly, the P375C substitution disrupted the transport function of TAP, leaving peptide binding unaffected. P375 caps coupling helix 2 by a kink, which may be important for signal transmission.

By oxidative cysteine cross-linking, we verified direct contacts between the CLs and the X-loop, thus providing evidence for domain swapping and dynamic transmission interface in the TAP complex. Based on the number of efficiently cross-linked residues, CL1 was found to be more flexible than CL2. However, it should be mentioned that CL1 is in close proximity not only to the X-loop of the opposite NBD but also to the Q-loop of the NBD in *cis* as demonstrated by chemical cross-linking studies using the multidrug exporter BmrA of *B. subtilis* (39). On the other hand, CL2 does not exclusively form contacts with the X-loop but also with the Q-loop of the *trans* NBD as shown by chemical cross-linking for P-gp and CFTR (30, 31, 40). A similar Sav1866-like interdomain organization was recently found for the yeast ABC exporter Yor1p (41).

The transmission interface, framed by the CLs and the NBDs, showed considerable flexibility because we detected a similar cross-linking pattern in the presence of ATP, peptides, ATP plus AlF_x, or the viral inhibitor ICP47 (Fig. S4). A highly dynamic arrangement of the transmission interface was also recently observed for CFTR (22, 30, 31). The need for conformational changes in the transmission interface during the transport cycle is supported by transport inhibition through cross-linking of the CLs with the NBDs. In BmrA, cross-linking of CL1 with the Q-loop of the NBD in *cis* disrupted ATP hydrolysis and substrate transport (39). Arresting CFTR by chemical cross-linking of CL2 or CL4 with residues near the Q-loop of the *trans* NBD impaired channel activity (30, 31). Here, we demonstrate that cross-linking of CL1 with the X-loop in *trans* arrested the TAP complex in a transport-incompetent state, which could, however, still bind peptides. The transmission interface is not restricted to a narrow region of the polypeptide chain but rather is distributed among the NBDs and CLs of the TMDs. Notably, cross-linking of CL2 in TAP1 and the X-loop in TAP2 impaired not only transport but also peptide binding. Because CL2 is part of the peptide-binding pocket, it is likely that the disulfide bridge inactivates the peptide-binding pocket by structural restrains. Thus, the CLs have different functions in substrate binding, signaling, and translocation.

Materials and Methods

Additional procedures are detailed in *SI Materials and Methods*.

Homology Modeling of the Core TAP Transport Complex. Each TAP1 and TAP2 half-transporter was modeled on the corresponding subunit of the ADP-bound *S. aureus* Sav1866 homodimer (PDB ID code 2HYD) (22). Although the Sav1866 structure was crystallized with ADP, the tight NBD dimer conformation and outward-facing configuration of the TMDs is believed to represent the ATP-bound state (22). The Sav1866 conformation allowed us to develop a homology

BIOCHEMISTRY

model of heterodimeric TAP complex in the ATP-bound state. We aligned the amino acid sequence of human TAP1 and TAP2 with that of Sav1866 using ClustalW2 (42). Secondary structure predictions (43) and experimental data on the membrane topology (26) for the TAP1 and TAP2 TM helices corresponded to the Sav1866-based alignment. The alignment for core TAP1 (173–741) and TAP2 (141–686), respectively, against Sav1866 revealed 27% and 28% sequence identity, although this varies markedly between the TMDs and NBDs. The sequence identity between core TAP1 and Sav1866 is 20% for the TMDs and 37% for the NBDs. For the alignment between core TAP2 and Sav1866, the sequence identity is 22% for the TMDs and 34% for the NBDs. When sequence similarity is taken into account, these percentages turn to 61% and 56% for the TMDs and to 69% and 63% for the NBDs of TAP1 and TAP2, respectively. TAP1 and TAP2 were modeled separately by means of MODELLER v9.3 (44). The TAP1 and TAP2 models were dimerized to reproduce the Sav1866 subunit interface and refined to remove steric clashes (45). The models were inserted into a 1-palmitoyl-2-oleoyl-*sn*-glycero-3-phosphoethanolamine lipid bilayer, and the system was solvated (24). Position restraints on the protein backbone conformation were relaxed over a 40-ps period by using the GROMACS 3.2.1 simulation package to give an energy minimized TAP1/2 heterodimer.

Cysteine Cross-Linking. TAP-containing membranes (0.5 mg of total protein) were incubated with CuPhe (1 mM $CuSO_4$/4 mM 1,10-phenanthroline; Sigma) in 100 μl of PBS (pH 7.4) for 1 min at 4 °C. The reaction was stopped by addition of 10 mM *N*-ethylmaleimide (NEM; Sigma). The membranes were washed with 500 μl of reaction buffer containing 10 mM EDTA and collected by centrifugation at 20,000 $\times$ *g* for 8 min at 4 °C. The membranes were resuspended in SDS-sample buffer containing 10 mM NEM and were analyzed by nonreducing 6% SDS/PAGE and immunoblotting with mAbs anti-TAP1 (mAb 148.3) (25) and anti-TAP2 (mAb 435.3) (17). For cleavage of the cross-linked disulfide bonds, 100 mM of DTT was added to the sample buffer before electrophoresis. To test the effect of cross-linking on TAP function, the membranes were treated with or without CuPhe for 1 min at 4 °C. Thereafter, the membranes were incubated with or without 100 mM of 2-mercaptoethanol for 5 min at 4 °C and washed twice with 1 ml of PBS containing 10 mM EDTA. Peptide binding and transport was analyzed as described above.

ACKNOWLEDGMENTS. We thank Gudrun Illig and Eckhard Linker for excellent technical assistance and Drs. David Parcej and Dirk Schiller for helpful comments. G.O. was a fellow of the International Max Planck Research School. M.L.O. was supported by a fellowship from the Canadian Institutes of Health Research. W.F.D.B. was supported by studentships from the Alberta Heritage Foundation for Medical Research and the Natural Science and Engineering Research Council. This work was supported by the Canadian Institutes of Health Research (D.P.T.) and German Research Foundation Grant SFB 807 (to R.T.) and Ab 149 (to R.A. and R.T.). D.P.T. is an Alberta Heritage Foundation for Medical Research Senior Scholar and Canadian Institutes of Health Research New Investigator. R.T. is principle investigator of the Cluster of Excellence Frankfurt–Macromolecular Complexes.

1. Abele R, Tampé R (2004) The ABCs of immunology: Structure and function of TAP, the transporter associated with antigen processing. *Physiology* 19:216–224.
2. Groothuis T, Neefjes J (2005) The ins and outs of intracellular peptides and antigen presentation by MHC class I molecules. *Curr Top Microbiol Immunol* 300:127–148.
3. Peaper DR, Cresswell P (2008) Regulation of MHC class I assembly and peptide binding. *Annu Rev Cell Dev Biol* 24:343–368.
4. Schmitt L, Tampé R (2002) Structure and mechanism of ABC transporters. *Curr Opin Struct Biol* 12:754–760.
5. Hollenstein K, Dawson RJ, Locher KP (2007) Structure and mechanism of ABC transporter proteins. *Curr Opin Struct Biol* 17:412–418.
6. Dean M, Annilo T (2005) Evolution of the ATP-binding cassette (ABC) transporter superfamily in vertebrates. *Annu Rev Genomics Hum Genet* 6:123–142.
7. Davidson AL, Dassa E, Orelle C, Chen J (2008) Structure, function, and evolution of bacterial ATP-binding cassette systems. *Microbiol Mol Biol Rev* 72:317–364.
8. Smith PC, et al. (2002) ATP binding to the motor domain from an ABC transporter drives formation of a nucleotide sandwich dimer. *Mol Cell* 10:139–149.
9. Fetsch EE, Davidson AL (2002) Vanadate-catalyzed photocleavage of the signature motif of an ATP-binding cassette (ABC) transporter. *Proc Natl Acad Sci USA* 99:9685–9690.
10. Chen J, Lu G, Lin J, Davidson AL, Quiocho FA (2003) A tweezers-like motion of the ATP-binding cassette dimer in an ABC transport cycle. *Mol Cell* 12:651–661.
11. Zaitseva J, Jenewein S, Jumpertz T, Holland IB, Schmitt L (2005) H662 is the linchpin of ATP hydrolysis in the nucleotide-binding domain of the ABC transporter HlyB. *EMBO J* 24:1901–1910.
12. Janas E, et al. (2003) The ATP hydrolysis cycle of the nucleotide-binding domain of the mitochondrial ATP-binding cassette transporter Mdl1p. *J Biol Chem* 278:26862–26869.
13. Koch J, Guntrum R, Heintke S, Kyritsis C, Tampé R (2004) Functional dissection of the transmembrane domains of the transporter associated with antigen processing (TAP). *J Biol Chem* 279:10142–10147.
14. Koch J, Guntrum R, Tampé R (2005) Exploring the minimal functional unit of the transporter associated with antigen processing. *FEBS Lett* 579:4413–4416.
15. Procko E, Raghuraman G, Wiley DC, Raghavan M, Gaudet R (2005) Identification of domain boundaries within the N-termini of TAP1 and TAP2 and their importance in tapasin binding and tapasin-mediated increase in peptide loading of MHC class I. *Immunol Cell Biol* 83:475–482.
16. Leonhardt RM, Keusekotten K, Bekpen C, Knittler MR (2005) Critical role for the tapasin-docking site of TAP2 in the functional integrity of the MHC class I-peptide-loading complex. *J Immunol* 175:5104–5114.
17. van Endert PM, et al. (1994) A sequential model for peptide binding and transport by the transporters associated with antigen processing. *Immunity* 1:491–500.
18. Gorbulev S, Abele R, Tampé R (2001) Allosteric crosstalk between peptide-binding, transport, and ATP hydrolysis of the ABC transporter TAP. *Proc Natl Acad Sci USA* 98:3732–3737.
19. Nijenhuis M, Hämmerling GJ (1996) Multiple regions of the transporter associated with antigen processing (TAP) contribute to its peptide binding site. *J Immunol* 157:5467–5477.
20. Herget M, et al. (2007) Mechanism of substrate sensing and signal transmission within an ABC transporter: Use of a Trojan horse strategy. *J Biol Chem* 282:3871–3880.
21. Neumann L, Abele R, Tampé R (2002) Thermodynamics of peptide binding to the transporter associated with antigen processing (TAP). *J Mol Biol* 324:965–973.
22. Dawson RJ, Locher KP (2006) Structure of a bacterial multidrug ABC transporter. *Nature* 443:180–185.
23. Ward A, Reyes CL, Yu J, Roth CB, Chang G (2007) Flexibility in the ABC transporter MsbA: Alternating access with a twist. *Proc Natl Acad Sci USA* 104:19005–19010.
24. O'Mara ML, Tieleman DP (2007) P-glycoprotein models of the apo and ATP-bound states based on homology with Sav1866 and MalK. *FEBS Lett* 581:4217–4222.
25. Schrodt S, Koch J, Tampé R (2006) Membrane topology of the transporter associated with antigen processing (TAP1) within an assembled functional peptide-loading complex. *J Biol Chem* 281:6455–6462.
26. Meyer TH, van Endert PM, Uebel S, Ehring B, Tampé R (1994) Functional expression and purification of the ABC transporter complex associated with antigen processing (TAP) in insect cells. *FEBS Lett* 351:443–447.
27. Ritz U, et al. (2001) Identification of sequences in the human peptide transporter subunit TAP1 required for transporter associated with antigen processing (TAP) function. *Int Immunol* 13:31–41.
28. Wu J, Kaback HR (1996) A general method for determining helix packing in membrane proteins in situ: Helices I and II are close to helix VII in the lactose permease of Escherichia coli. *Proc Natl Acad Sci USA* 93:14498–14502.
29. Guan L, Kaback HR (2006) Lessons from lactose permease. *Annu Rev Biophys Biomol Struct* 35:67–91.
30. Serohijos AW, et al. (2008) Phenylalanine-508 mediates a cytoplasmic-membrane domain contact in the CFTR 3D structure crucial to assembly and channel function. *Proc Natl Acad Sci USA* 105:3256–3261.
31. He L, et al. (2008) Multiple membrane-cytoplasmic domain contacts in the Cystic Fibrosis Transmembrane Conductance Regulator (CFTR) mediate regulation of channel gating. *J Biol Chem* 283:26383–26390.
32. Loo TW, Bartlett MC, Clarke DM (2008) Processing mutations disrupt interactions between the nucleotide binding and transmembrane domains of P-glycoprotein and the cystic fibrosis transmembrane conductance regulator (CFTR). *J Biol Chem* 283:28190–28197.
33. Careaga CL, Falke JJ (1992) Thermal motions of surface alpha-helices in the D-galactose chemosensory receptor. Detection by disulfide trapping. *J Mol Biol* 226:1219–1235.
34. Antoniou AN, Ford S, Pilley ES, Blake N, Powis SJ (2002) Interactions formed by individually expressed TAP1 and TAP2 polypeptide subunits. *Immunology* 106:182–189.
35. Keusekotten K, Leonhardt RM, Ehses S, Knittler MR (2006) Biogenesis of functional antigenic peptide transporter TAP requires assembly of pre-existing TAP1 with newly synthesized TAP2. *J Biol Chem* 281:17545–17551.
36. Neumann L, Tampé R (1999) Kinetic analysis of peptide binding to the TAP transport complex: Evidence for structural rearrangements induced by substrate binding. *J Mol Biol* 294:1203–1213.
37. Lewis HA, et al. (2004) Structure of nucleotide-binding domain 1 of the cystic fibrosis transmembrane conductance regulator. *EMBO J* 23:282–293.
38. Schmitt L, Benabdelhak H, Blight MA, Holland IB, Stubbs MT (2003) Crystal structure of the nucleotide-binding domain of the ABC-transporter haemolysin B: Identification of a variable region within ABC helical domains. *J Mol Biol* 330:333–342.
39. Dalmas O, et al. (2005) The Q-loop disengages from the first intracellular loop during the catalytic cycle of the multidrug ABC transporter BmrA. *J Biol Chem* 280:36857–36864.
40. Zolnerciks JK, Wooding C, Linton KJ (2007) Evidence for a Sav1866-like architecture for the human multidrug transporter P-glycoprotein. *FASEB J* 21:3937–3948.
41. Pagant S, Brovman EY, Halliday JJ, Miller EA (2008) Mapping of interdomain interfaces required for the functional architecture of Yor1p, a eukaryotic ATP-binding cassette (ABC) transporter. *J Biol Chem* 283:26444–26451.
42. Thompson JD, Higgins DG, Gibson TJ (1994) CLUSTAL W: Improving the sensitivity of progressive multiple sequence alignment through sequence weighting, position-specific gap penalties and weight matrix choice. *Nucleic Acids Res* 22:4673–4680.
43. Rost B, Yachdav G, Liu J (2003) The PredictProtein server. *Nucleic Acids Res* 32:W321–W326.
44. Sali A, Blundell TL (1993) Comparative protein modelling by satisfaction of spatial restraints. *J Mol Biol* 234:779–815.
45. Guex N, Peitsch MC (1997) SWISS-MODEL and the Swiss-PdbViewer: An environment for comparative protein modeling. *Electrophoresis* 18:2714–2723.

Supporting Information

Oancea et al. 10.1073/pnas.0811260106

SI Materials and Methods

Sequence Alignment and Secondary Structure Prediction. The quality of a homology model is governed directly by the accuracy of the sequence alignment. In low sequence identity regions such as the transmembrane domain (TMD), an inaccurate sequence alignment potentially alters the residue distribution of the translocation pore and the interhelical contact points that enable functional regions of TAP1/2 to be identified from the homology model. Secondary structure predictions were previously performed on TAP1 and TAP2 to pin down the location of membrane spanning helices (1), improving the quality of the sequence alignment in this region. The Sav1866 crystal structure contains 15 helical segments in the TMD alone, arranged into 6 transmembrane helices that extend up to 35 Å into the cytoplasm, coupling with the nucleotide-binding domains (NBDs) (2). To demarcate the membrane embedded regions of each helix, secondary structure predictions were performed on the Sav1866 primary sequences using 4 different transmembrane helix (TM) prediction servers (SOSUI, TMHMM, TopPRED2, and TMpred) (3–6). To verify the secondary structure predictions, the membrane spanning regions of the Sav1866 were also identified from a 1-palmitoyl-2-oleoyl-*sn*-glycero-3-phosphoethanolamine (POPE) embedded, solvated, and equilibrated Sav1866 crystal structure (PDB ID code 2HYD). These were compared to the TAP1 and TAP2 secondary structure predictions and experimentally determined membrane-spanning segments (1). Although the predictions do not precisely concur with the experimental predictions, the experimental TAP1/2 and modeled Sav1866 helix demarcations concur, and the location of the predicted TM helices correlated with the secondary structure alignment, increasing our confidence in the TMD sequence alignment.

Construction and Expression of Mutants. Single cysteine TAP1 mutants of cytosolic loop 1 (CL1) (T273C, E274C, F275C, Q278C, and N279C) and of CL2 (I368C, E369C, A370C, P375C, T376C, V377C, R378C, S379C, F380C, A381C, and N382C) were generated by ligase chain reaction with the following primers using Cys-less human TAP1 with a C-terminal His_{10}-tag as template (1): T273C, CGTCCTGAGACAGGAATGCGAATTCTTCCA; E274C, GACAGGAAACCTGCTTCTTCCAGCAGAAC; F275C, AACCGAATTCTGCCAGCAGAACCAGAC; Q278C, GAATTCTTCCAGTGCAACCAGACCGGCAACAT; N279C, TTCTTCCAGCAGTGCCAGACCGGCAACAT; I368C, CCCAGGTCGCTTGCGAAGCCTTAAGTG; E369C, CAGGTCGCTATCTGCGCCTTAAGTGCTA; A370C, GGTCGCTATC GAATGCTTAAGTGCTATGCC; P375C, GCCTTAAGTGCTATGTGTACCGTCAGATC C; T376C, GTGCTATGCCTTGCGTCAGATCCTTC; V377C, TGCTATGCCTACCTGC AGATCCTTCGCTAA; R378C, TATGCCTACCGTCTGCTCCTTCGCTA AC; S379C, CCTACCGTCAGATGCTTCGCTAACGAAGA; F380C, TACCGTCAGATCCTGCGCT AACGAAGAAG; A381C, CAGATCCTTCTGTAACGAAGAAGGCGAAGCTC; N382C, AGATCCTTCGCTTGCGAAGAGGCGAAGCTC (exchanged nucleotides are underlined). The single cysteine TAP1 mutants Q277C, G282C, N283C, I284C, M285C, S286C, R287C, and V288C were generated by ligase chain reaction as described (7). The single cysteine TAP1 mutants of the CL1 were cloned in the BspTI and MluI sites of pFastBac1_TAP1(Cys-less), whereas the single-cysteine TAP1 mutants of the CL2 were cloned in the SphI and StuI sites of pFastBac1_TAP1(Cys-less). The conserved E602 in the X-loop of TAP2 was mutated by ligase chain reaction with the following primers using single-cysteine TAP2(C213) as template: E602C, TACACCGATGTCGGCTGCAAGGGCTCCCAACTG; E602R, CCGAT GTCGGCAGAAAGGGCTCCCAACT; E602D, CCGATGTCGGCGATAAGGGCTCCCA ACT; E602A, TACACCGATGTCGGCGCTAAGGGCTCCCAACT. The X-loop mutants of TAP2 were cloned in the AjiI and AatII sites of pFasBac1-TAP2(C213). All enzymes for cloning were purchased from Fermentas. The constructs were confirmed by DNA sequencing. Baculovirus generation, virus infection, and protein expression were performed as previously described (8). Coinfections with baculoviruses containing single-cysteine TAP1 mutants and single-cysteine TAP2 (X-loop) were performed with a multiplicity of infection of 5. Infections with baculovirus containing Cys-less TAP1 in combination with Cys-depleted TAP2 were performed at a multiplicity of infection of 3 (1). TAP-containing membranes were prepared as previously described (7). The protein concentration was determined by the MicroBCA assay (Pierce).

Peptide Binding Assay. Peptides were radiolabeled with iodine (^{125}I) (8). TAP-containing membranes (25 μg of total protein) were incubated with 1 μM of radio-labeled peptide RRYQKSTEL in 50 μl of binding buffer (5 mM $MgCl_2$ in PBS, pH 7.4) for 15 min at 4 °C. Unbound peptides were removed by washing the membranes twice with 100 μl of ice-cold binding buffer using a vacuum manifold with 96-well filter plates (0.65 μm of polyvinylidene difluoride membranes, MultiScreen; Millipore). Membrane-associated radioactivity was quantified by γ-counting. Background binding was determined in the presence of 200-fold excess of unlabeled peptide (RRYQKSTEL).

Peptide Transport Assay. TAP-containing membranes (150 μg of total protein) were resuspended in 50 μl of binding buffer in the presence of 3 mM ATP or 2 units of apyrase. The transport reaction (50 μl) was started by adding 1 μM of fluorescent peptide RRYQNSTC$^{(F)}$L [$^{(F)}$, fluorescein-labeled cysteine] for 5 min at 32 °C and terminated with stop buffer (10 mM EDTA in PBS, pH 7.4) on ice (9). After centrifugation, the membranes were solubilized in lysis buffer (50 mM Tris/HCl, 150 mM NaCl, 5 mM KCl, 1 mM $CaCl_2$, 1 mM $MnCl_2$, 1% Nonidet P-40, pH 7.4) for 20 min on ice. N-core glycosylated, and therefore transported peptides were recovered overnight at 4 °C with Con A Sepharose beads (Sigma). After washing with lysis buffer, glycosylated peptides were eluted with 200 mM methyl-α-D-mannopyranoside (Sigma) in lysis buffer and quantified with a fluorescence plate reader ($\lambda_{ex/em}$ = 485/520 nm, Polarstar Galaxy; BMG Labtech).

1. Schrodt S, Koch J, Tampé R (2006) Membrane topology of the transporter associated with antigen processing (TAP1) within an assembled functional peptide-loading complex. *J Biol Chem* 281:6455–6462.
2. Dawson RJ, Locher KP (2006) Structure of a bacterial multidrug ABC transporter. *Nature* 443:180–185.
3. Hirokawa T, Boon-Chieng S, Mitaku S (1998) SOSUI: classification and secondary structure prediction system for membrane proteins. *Bioinformatics* 14:378–379.
4. Krogh A, Larsson B, von Heijne G, Sonnhammer EL (2001) Predicting transmembrane protein topology with a hidden Markov model: Application to complete genomes. *J Mol Biol* 305:567–580.

5. von Heijne G (1992) Membrane protein structure prediction. Hydrophobicity analysis and the positive-inside rule. *J Mol Biol* 225:487–494.
6. Hofmann K, Stoffel W (1993) TMbase - A database of membrane spanning proteins segments. *Biol Chem Hoppe-Seyler* 374:166–166.
7. Herget M, et al. (2007) Mechanism of substrate sensing and signal transmission within an ABC transporter: Use of a Trojan horse strategy. *J Biol Chem* 282:3871–3880.
8. Chen M, Abele R, Tampé R (2003) Peptides induce ATP hydrolysis at both subunits of the transporter associated with antigen processing. *J Biol Chem* 278:29686–29692.
9. Neumann L, Tampé R (1999) Kinetic analysis of peptide binding to the TAP transport complex: Evidence for structural rearrangements induced by substrate binding. *J Mol Biol* 294:1203–1213.

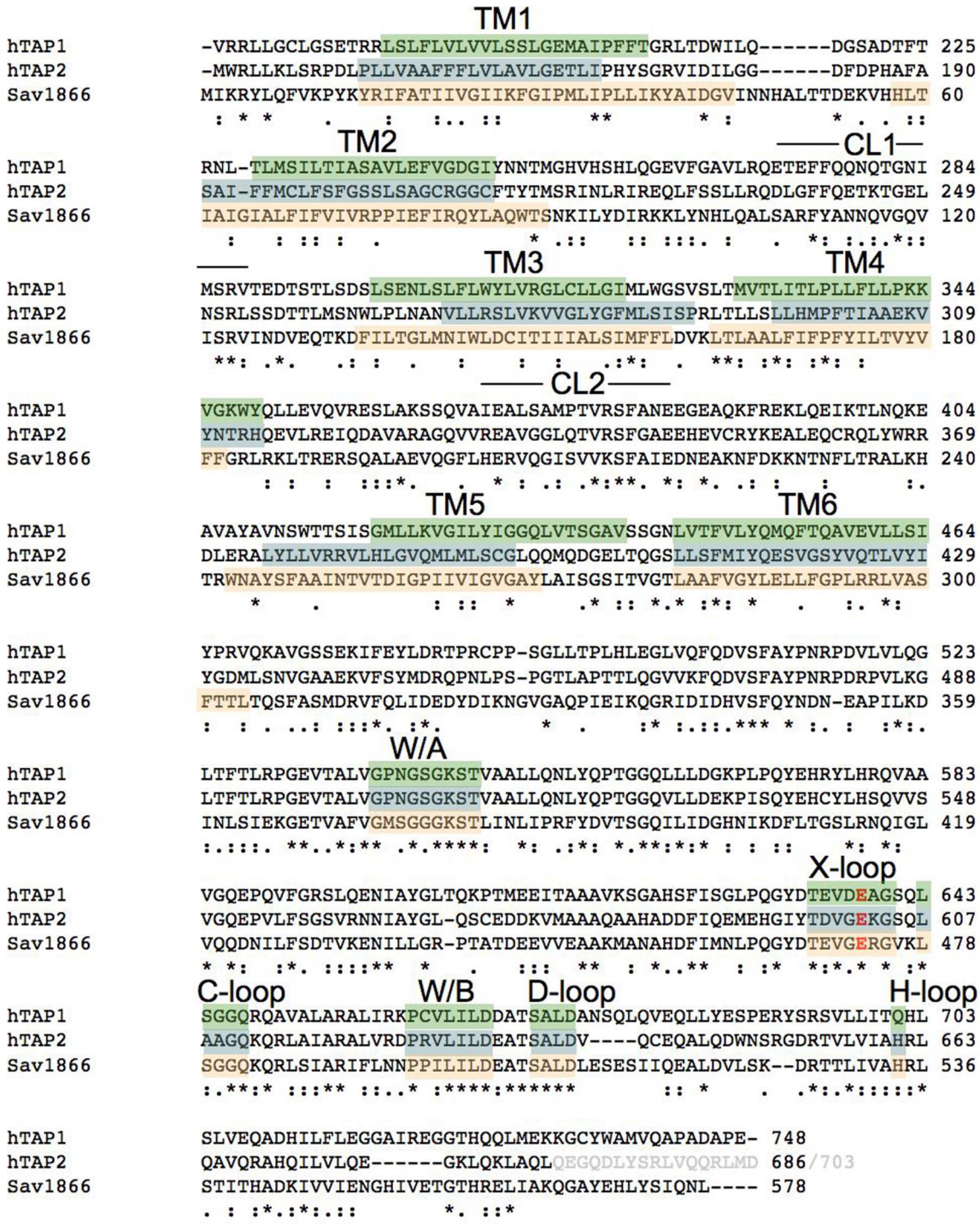

Fig. S1. Sequence alignment, membrane topology, and structural organization of TAP1, TAP2, and Sav1866. ClustalW2 was used for sequence alignment of human TAP1 (PDB ID code gi:45181465), TAP2 (PDB ID code gi:34638), and Sav1866 (PDB ID code gi:15924856). To verify the secondary structure predictions, the TM regions of the Sav1866 (orange) were also identified from a POPE embedded, solvated, and equilibrated Sav1866 structure (PDB ID code 2HYD) (2). These were compared to the TAP1 and TAP2 secondary structure predictions and experimentally determined membrane spanning segments (green and cyan) (1). Characteristic motifs and loops are indicated. The conserved glutamate residues of the X-loop are illustrated in red. The short (686 aa; PDB ID code gi:34638) and long TAP2 alleles [703 aa; PDB ID code gi:168985572 (gray)] are shown.

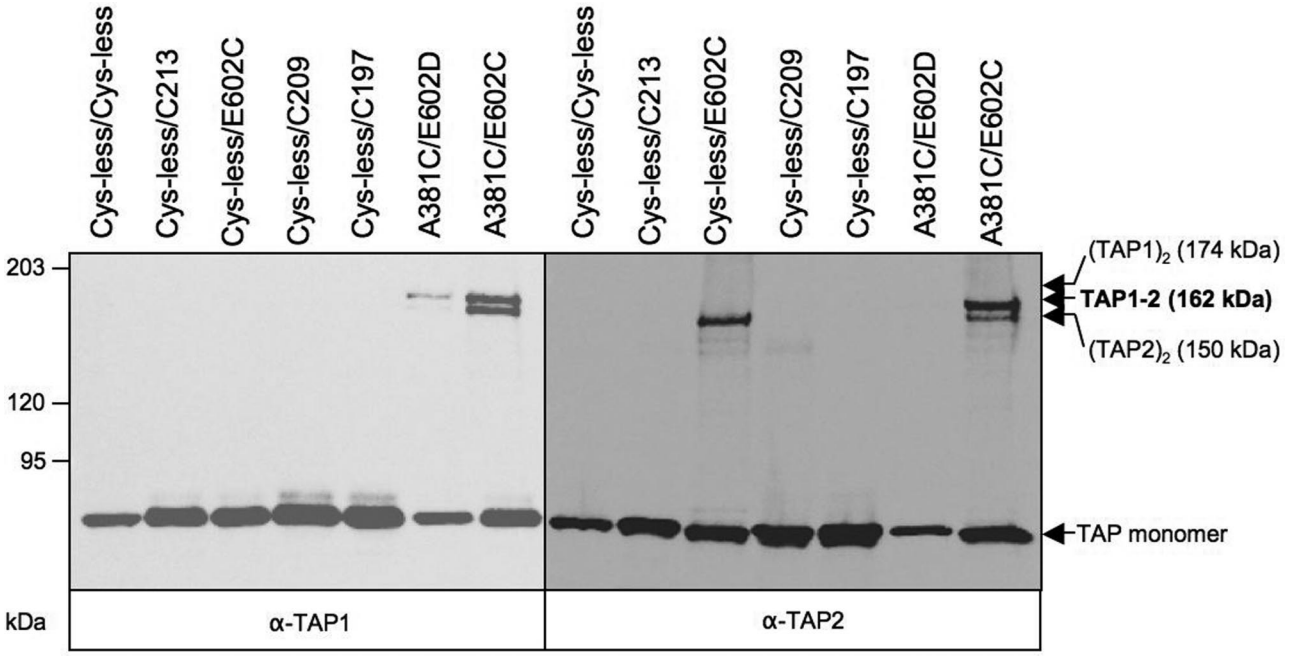

Fig. S2. Specific cross-linking between the cytosolic loops of TAP1 and the X-loop of TAP2. TAP-containing membranes (500 μg of total protein) were incubated in the presence or absence of 1 mM copper phenanthroline (CuPhe) for 1 min at 4 °C. Oxidative cross-linking was terminated by 10 mM each of *N*-ethylmaleimide (NEM) and EDTA. Samples were subjected to nonreducing 6% SDS/PAGE (20 μg of protein per lane) followed by immunoblotting against TAP1 and TAP2. The positions of the cross-linked TAP1–TAP2 (highlighted in bold), homodimeric $(TAP1)_2$ and $(TAP2)_2$ and monomeric TAP1 and TAP2 are indicated.

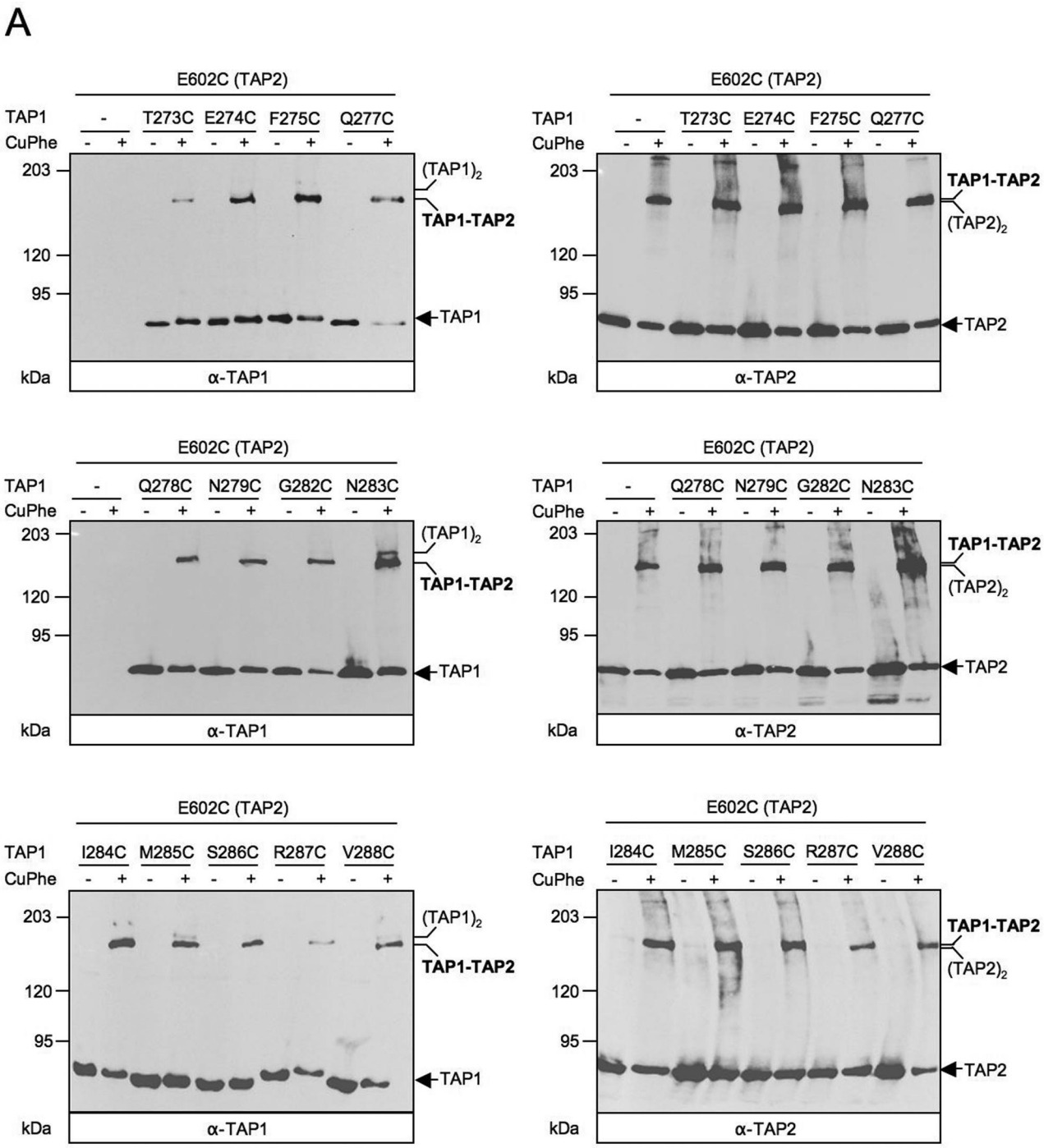

Fig. S3. Cysteine cross-linking between CL1 and CL2 of TAP1 and X-loop of TAP2. (*A* and *B*) The membranes (500 μg of protein) containing different single cysteine variants of the CL1 (*A*) and CL2 (*B*) of TAP1 and TAP2(E602C) were incubated in the presence or absence of 1 mM CuPhe for 1 min at 4 °C. Oxidative cross-linking was terminated by 10 mM each of NEM and EDTA. Samples were subjected to nonreducing 6% SDS/PAGE (20 μg of protein per lane) followed by immunoblotting against TAP1 and TAP2.

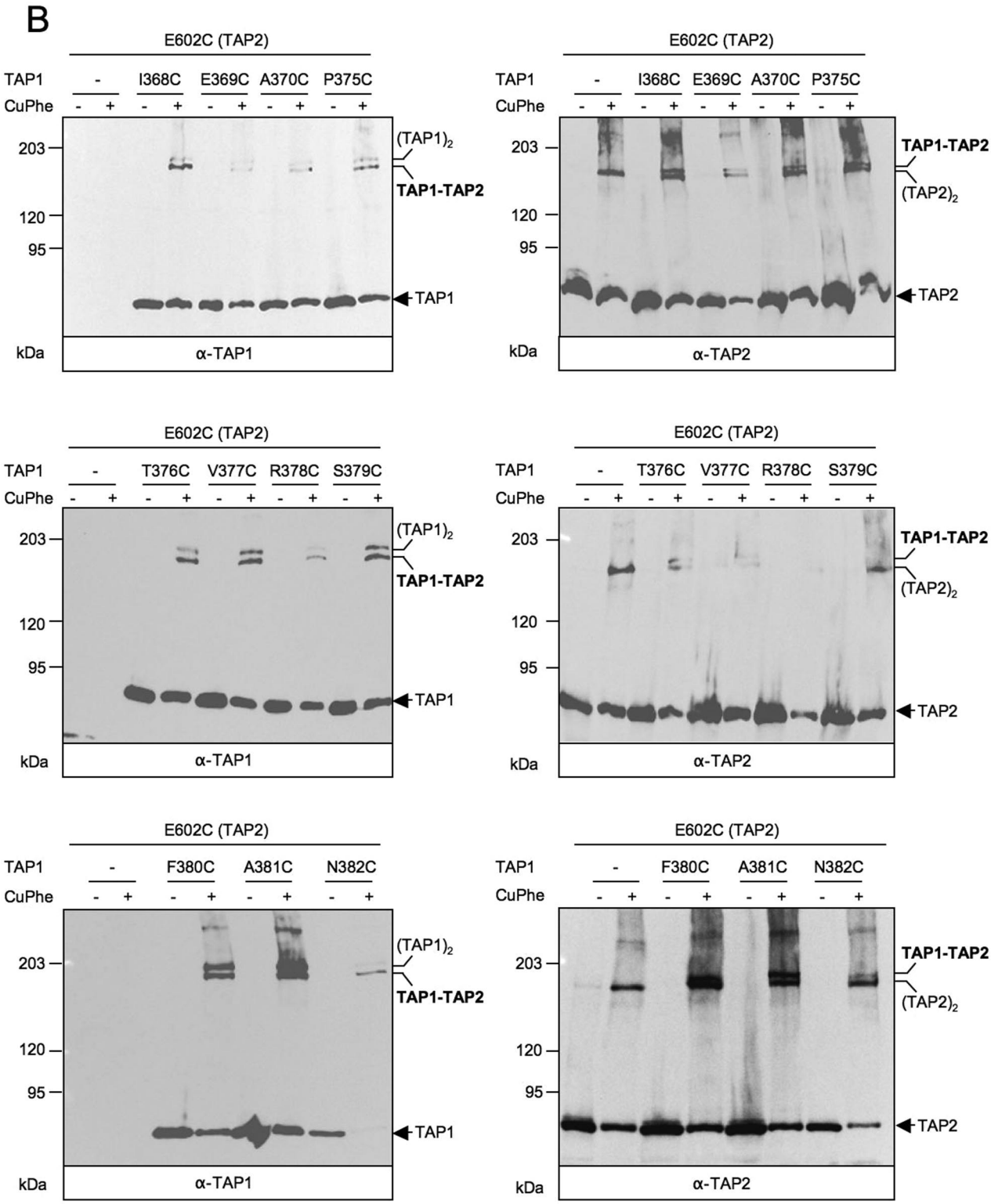

Fig. S3. continued.

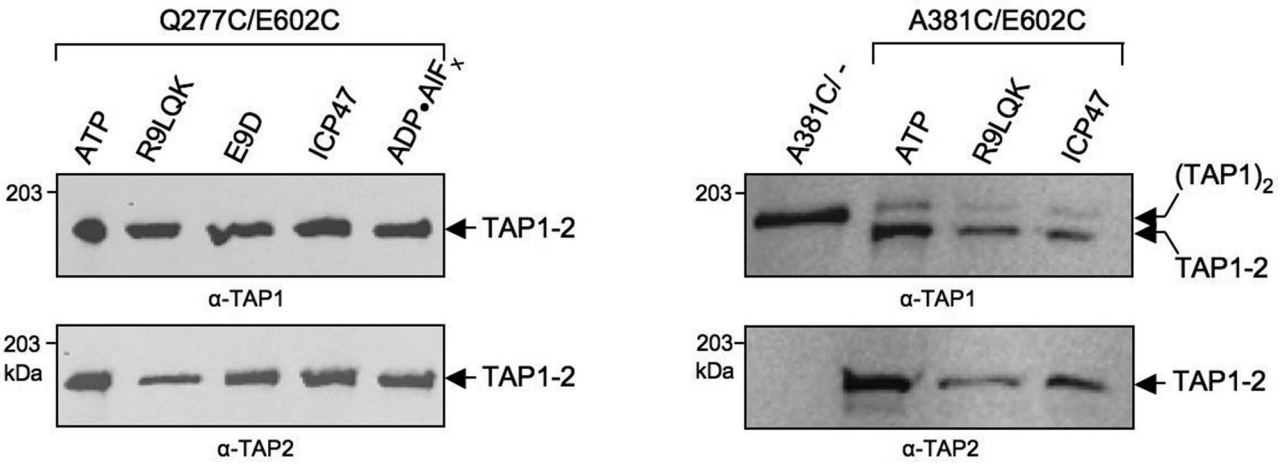

Fig. S4. Cross-linking efficiency between the X-loop and CL1 or CL2 remains stable at various stages of the transport cycle. TAP-containing membranes (500 μg of protein) were incubated with either 10 mM ATP, 10 μM R9LQK, 10 μM E9D (nonbinder), or 10 μM ICP47 for 25 min at 27 °C. For nucleotide trapping, TAP-containing membranes were preincubated with 1 μM RRYQKSTEL (R9LQK) and 5 mM ATP in the presence of 2.5 mM AlF_x for 25 min at 27 °C. Afterward, oxidative cross-linking was initiated in the presence of 1 mM CuPhe for 1 min at 4 °C. Oxidative cross-linking was terminated by 10 mM each of NEM and EDTA. After metal affinity capture of TAP, cross-linked products were analyzed by nonreducing 6% SDS/PAGE followed by immunoblotting against TAP1 and TAP2. The positions of the cross-linked heterodimeric TAP1–2 and homodimeric $(TAP1)_2$ are indicated.

Table S1. CL/X-loop distances in different TAP1/2 models

TAP1/2 model based on	CL1 C_α distances for residues 277–602, Å	CL2 C_α distances for residues 381–602, Å
Sav1866 (PDB ID code 2HYD)	7.7	20.5
ADP-vanadate MsbA (PDB ID code 3B5Z)	7.0	21.0
closed apo MsbA (PDB ID code 2B5X)	26.5	25.6
open apo MsbA (PDB ID code 2B5W)	63.1	26.0